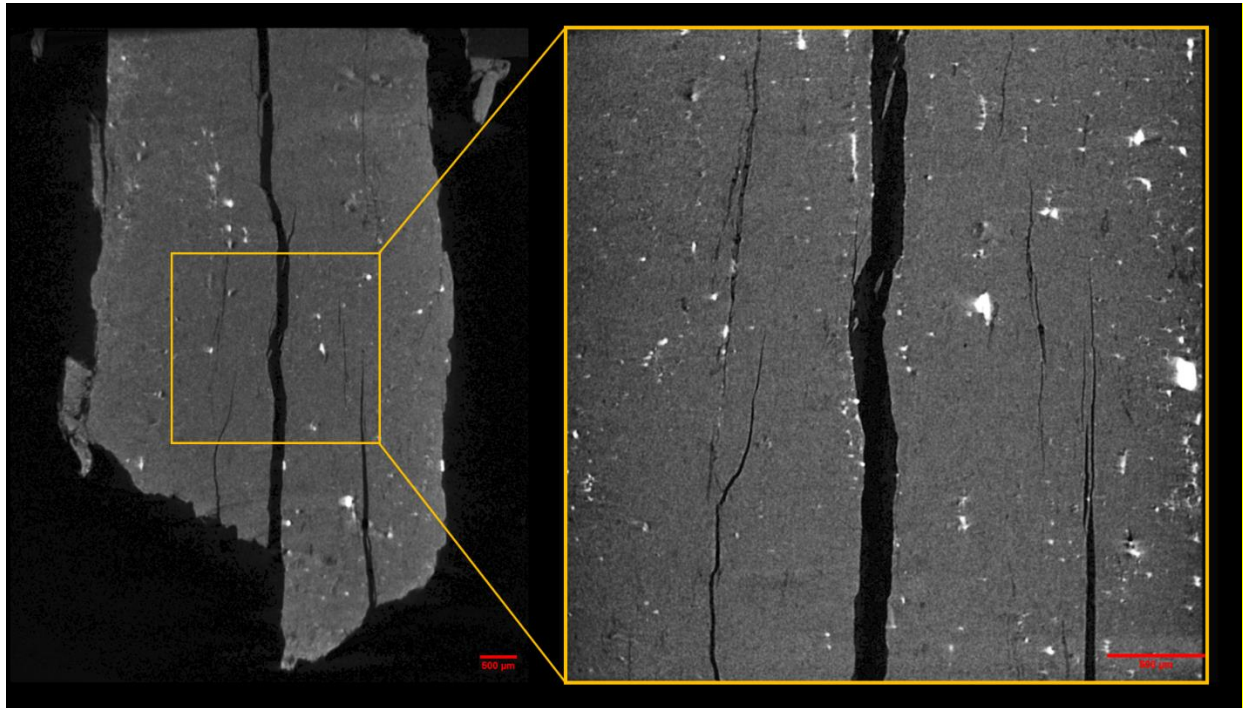


NETL

NATIONAL ENERGY TECHNOLOGY LABORATORY



Computed Tomography Scanning and Petrophysical Measurements of Eastern Williston Basin Twin Buttes and Hagel Formations

1 November 2024



Office of Fossil Energy and
Carbon Management

DOE/NETL-2025/4886

Disclaimer

This project was funded by the United States Department of Energy, National Energy Technology Laboratory, in part, through a site support contract. Neither the United States Government nor any agency thereof, nor any of their employees, nor the support contractor, nor any of their employees, makes any warranty, express or implied, or assumes any legal liability or responsibility for the accuracy, completeness, or usefulness of any information, apparatus, product, or process disclosed, or represents that its use would not infringe privately owned rights. Reference herein to any specific commercial product, process, or service by trade name, trademark, manufacturer, or otherwise does not necessarily constitute or imply its endorsement, recommendation, or favoring by the United States Government or any agency thereof. The views and opinions of authors expressed herein do not necessarily state or reflect those of the United States Government or any agency thereof.

Cover Illustration: Images from micro-computed tomography (CT) scans of a sample from the 23-B021 Well at a depth 141.95 ft showing fractures (black) and high-density minerals (white) in the Hagel formation. Left, scan with a resolution of 4.42 μm . Right, scan with a resolution of 1.68 μm . Scale bars are 500 μm .

Suggested Citation: Paronish, T.; Crandall, D.; Jarvis, K.; Workman, S.; Drosche, J.; Pohl, M.; Mckisic, T.; Feole, I.; Folkedahl, B.; Kay, J. *Computed Tomography Scanning and Petrophysical Measurements of Eastern Williston Basin Twin Buttes and Hagel Formations*; DOE/NETL-2024/4886; NETL Technical Report Series; U.S. Department of Energy, National Energy Technology Laboratory: Morgantown, WV, 2024; p 40.

An electronic version of this report can be found at:

<https://edx.netl.doe.gov/group/core-characterization>

<https://netl.doe.gov/energy-analysis/search>

The data in this report can be accessed from NETL's Energy Data eXchange ([EDX](#)) online system (<https://edx.netl.doe.gov>) using the following link:

https://edx.netl.doe.gov/dataset/eerc_corecm_williston_basin_cores

Computed Tomography Scanning and Petrophysical Measurements of Eastern Williston Basin Twin Buttes and Hagel Formations

Thomas Paronish^{1,2}; Dustin Crandall¹; Karl Jarvis^{1,2}; Scott Workman^{1,2}; Jessica Drosche^{1,2}; Mathias Pohl^{1,2}; Terry Mckisic^{1,2}; Ian Foele³; Bruce Folkedahl³; John Kay³

**¹National Energy Technology Laboratory, 3610 Collins Ferry Road, Morgantown, WV
26505, USA**

²NETL Support Contractor, 3610 Collins Ferry Road, Morgantown, WV 26505, USA

**³Energy and Environmental Research Center, University of North Dakota, 15 North 23rd
Street, Grand Forks, ND 58202-9018, USA**

DOE/NETL-2025/4886

1 November 2024

NETL Contacts:

Dustin Crandall, Principal Investigator

R. Burt Thomas, Technical Portfolio Lead

Bryan Morreale, Associate Laboratory Director for Research & Innovation, Research &
Innovation Center

This page intentionally left blank.

Table of Contents

ABSTRACT	1
1. INTRODUCTION	2
1.1 SITE BACKGROUND.....	2
1.2 CORE DESCRIPTION.....	3
2. DATA ACQUISITION AND METHODOLOGY	7
2.1 MEDICAL CT SCANNING.....	7
2.2 INDUSTRIAL CT SCANNING.....	8
2.3 MICRO-CT SCANNING.....	8
2.4 CORE LOGGING.....	10
2.5 DATA COMPILATION.....	12
3. RESULTS	13
3.1 MEDICAL CT SCANS.....	13
3.2 ADDITIONAL CT DATA.....	17
3.3 DUAL ENERGY CT SCANNING.....	20
3.4 COMPILED CORE LOG.....	22
4. DISCUSSION	25
5. REFERENCES	27

List of Figures

Figure 1: Map of MC233080C and 23-B001 wells.	2
Figure 2: Core photos, medical CT images, and stratigraphic description for the MC23080C well.	4
Figure 3: Core photos, medical CT images, and stratigraphic description for the 23-B001 well (1 of 2).	5
Figure 4: Core photos, medical CT images, and stratigraphic description for the 23-B001 well (2 of 2).	6
Figure 5: Toshiba Aquilion Multislice Helical CT scanner at NETL used for core analysis.	7
Figure 6: North Star Imaging Inc. M-5000 ® Industrial CT Scanner at NETL used for core analysis.	8
Figure 7: TESCAN DynaTOM Micro-CT scanner used for high-resolution CT imaging at NETL.	9
Figure 8: Zeiss Xradia MicroXCT-400 Micro-CT scanner used for high-resolution CT imaging at NETL.	9
Figure 9: Periodic table showing elements measurable by the Olympus Vanta M Series XRF Spectrometer using the “GeoChem(3-beam)” mode.	12
Figure 10: Schematic of the XZ isolated plane through the vertical center of the medical CT scans.	13
Figure 11: 2D isolated planes through the vertical center of the medical CT scans of the 23-B001 well from 127–135 ft.	14
Figure 12: 2D isolated planes through the vertical center of the medical CT scans of the 23-B021 well from 135–142 ft.	15
Figure 13: 2D isolated planes through the vertical center of the medical CT scans of the MC23080C well from 34–42 ft.	16
Figure 14: Single image from a video file available on EDX showing variation in the MC23080C well core from 38–42 ft.	17
Figure 15: 2D isolated planes through the vertical center of the industrial CT scans of the 23-B001 well from 140.6 ft.	18
Figure 16: 2D isolated planes through the vertical center of the Xradia micro-CT scans of the 23-B001 well from 139 ft to 141.95 ft.	19
Figure 17: 2D isolated planes through the vertical center of the micro-CT scans of the 23-B001 well from 139.8 ft and 141 ft.	20
Figure 18: Photon interactions at varying energies: a) Photoelectric absorption, b) Compton scattering.	21
Figure 19: Compiled core log for the 23-B001 well from 127–142 ft.	23
Figure 20: Compiled core log for MC23080C well from 34–42 ft.	24

List of Tables

Table 1: Magnetic Susceptibility Values for Common Minerals	10
Table 2: Industrial Scans from Whole Core, All Available on EDX.....	17
Table 3: Overview of Available Micro-CT Scans, All Available on EDX	18
Table 4: DynaTOM Micro Scans, All Available on EDX.....	20
Table 5: Dual Energy Calibration Standards, Bulk Density (gm/cm ³).....	21
Table 6: Dual Energy Calibration Standards, HU and CTN for “Low” and “High” Energies.....	21

Acronyms, Abbreviations, and Symbols

Term	Description
2D	Two-dimensional
3D	Three-dimensional
CT	Computed tomography
CTN	CT number
d	Sample thickness
DOE	U.S. Department of Energy
EERC	Energy and Environment Research Center
EDX	NETL's Energy Data eXchange
HU	Hounsfield Unit
H	External magnetic field
I	Measured intensity
I_0	Source intensity
J	Magnetic response (per unit volume)
k	Volume susceptibility
MSCL	Multi-Sensor Core Logger
NETL	National Energy Technology Laboratory
REE	Rare earth elements
XRF	X-ray fluorescence
μ	Compton attenuation coefficient
ρ	Bulk density

Acknowledgments

This work was completed at the National Energy Technology Laboratory (NETL) with support from the U.S. Department of Energy's (DOE) Office of Fossil Energy Oil & Gas Program. The authors wish to acknowledge Bryan Morreale (NETL Research & Innovation Center), Jessica Mullins and Scott Montross (NETL Science & Technology Strategic Plans and Programs), and Anna Wendt (DOE Office of Fossil Energy and Carbon Management) for programmatic guidance, direction, and support.

Thank you to the staff of the Geologic Characterization, Analytics, and Modeling Laboratory at NETL for continued laboratory support.

This page intentionally left blank.

ABSTRACT

The computed tomography (CT) facilities and the Multi-Sensor Core Logger (MSCL) at the U.S. Department of Energy's (DOE) National Energy Technology Laboratory (NETL) in Morgantown, West Virginia, were used to characterize core from two wells that represent coal resources across North Dakota. These include the:

- MC23080C Well in Mercer County
- 23-B001 Well in Oliver County

The primary impetus of this work was to capture a detailed digital representation of the core from the MC23080C and 23-B001 Wells. The collaboration between the NETL and the Energy and Environment Research Center (EERC) enables other research entities to access information about this potential carbon ore, rare earth, and critical mineral resource plays in the Williston Basin. The resultant datasets are presented in this report and can be accessed from NETL's Energy Data eXchange (EDX) using the following link:

https://edx.netl.doe.gov/dataset/eerc_corecm_williston_basin_cores.

All equipment and techniques used were non-destructive, enabling future examinations and analyses to be performed on these cores. Fractures, discontinuities, and millimeter-scale features were readily detectable with the medical CT scanner acquired images. Imaging with the NETL medical CT scanner was performed on entire cores. Qualitative analysis of the medical CT images, coupled with X-ray fluorescence (XRF), gamma density, and magnetic susceptibility measurements from the MSCL were useful in identifying zones of interest for potential future analysis. Higher-resolution industrial and micro-CT images were acquired from selected zones along the depth of the core to visualize the structure in higher detail. The ability to quickly identify key areas for more detailed study with higher resolution will save time and resources in future studies. The combination of methods used provides a multi-scale analysis of the core, with the resulting macro- and micro-descriptions relevant to many subsurface energy-related examinations traditionally performed at NETL.

1. INTRODUCTION

Evaluation of coal basin strata for identification of critical minerals and rare earth elements (REE) is an essential part of fulfilling the nation’s goal of sustainable energy transition from fossil energy and builds a more robust accounting of national reserves. As part of this effort, this technical report provides non-destructive characterization of a potential resource utilizing computed tomography (CT) imaging and petrophysical measurements via the Multi-Sensor Core Logger (MSCL) at the U.S. Department of Energy’s (DOE) National Energy Technology Laboratory (NETL). While it is common for commercial entities to perform these characterizations, the resources necessary to conduct these analyses are not always available to the broader interest base, such as state agencies and research-based consortia. To meet the growing need for comprehensive and high-quality lithologic data for collaborative research initiatives, NETL uses available resources to develop a systematic approach for the evaluation of subsurface geological core materials.

The data is presented in several formats here and online at NETL’s Energy Data eXchange (EDX) (https://edx.netl.doe.gov/dataset/eerc_corecm_williston_basin_cores). These data are potentially useful for various analyses. However, little detailed analysis is presented in this report as the research objective was not to perform site characterizations, but rather to acquire the data for others to utilize and to create a digital representation of the core that could be preserved in perpetuity.

1.1 SITE BACKGROUND

The MC23080C and 23-B001 wells were drilled for coal mine resource evaluation in September and December 2023, respectively. The MC23080C well was drilled in Mercer County, North Dakota (Lat. 47°24'46.80"N, Long. 101°40'35.04"W, Figure 1) with a total depth of 220 ft. This report focuses on the Twin Buttes seam intersected by the MC23080C well from 36 to 46 ft. The 23-B001 well was drilled in Oliver County, North Dakota (Lat. 47° 6'18.62"N, Long. 101°20'49.53"W, Figure 1) with a total depth of 160 ft. This report focuses on the Hagel Formation intersected by the 23-B001 well from 127 to 142 ft.



Figure 1: Map of MC233080C and 23-B001 wells.

1.2 CORE DESCRIPTION

Both the MC23080C and 23-B001 wells are drilled for exploration of lignite seams in the Sentinel Butte Formation. The MC23080C well cored through the Twin Buttes lignite, a seam that overlies the Beulah-Zap seam and is mined in the nearby Freedom Mine. The Twin Buttes lignite in the MC23080C well is between two claystone layers, the lignite has pyrite throughout and few calcite veins. A complete description and core photos are shown in Figure 2. The 23-B001 well is cored through the Hagel lignite seam. The Hagel seam is the lower most lignite that is mined in the nearby Center Mine. The Hagel lignite in the 23-B001 well is made up of approximately 8.4 ft lignite within the cored interval with 1-to-2-in. beds of claystone intervals at the base. The lignite is overlain by claystone and a 1-ft interval of lignite (Figure 3 and Figure 4).

Twin Buttes Coal - MC23080C Well

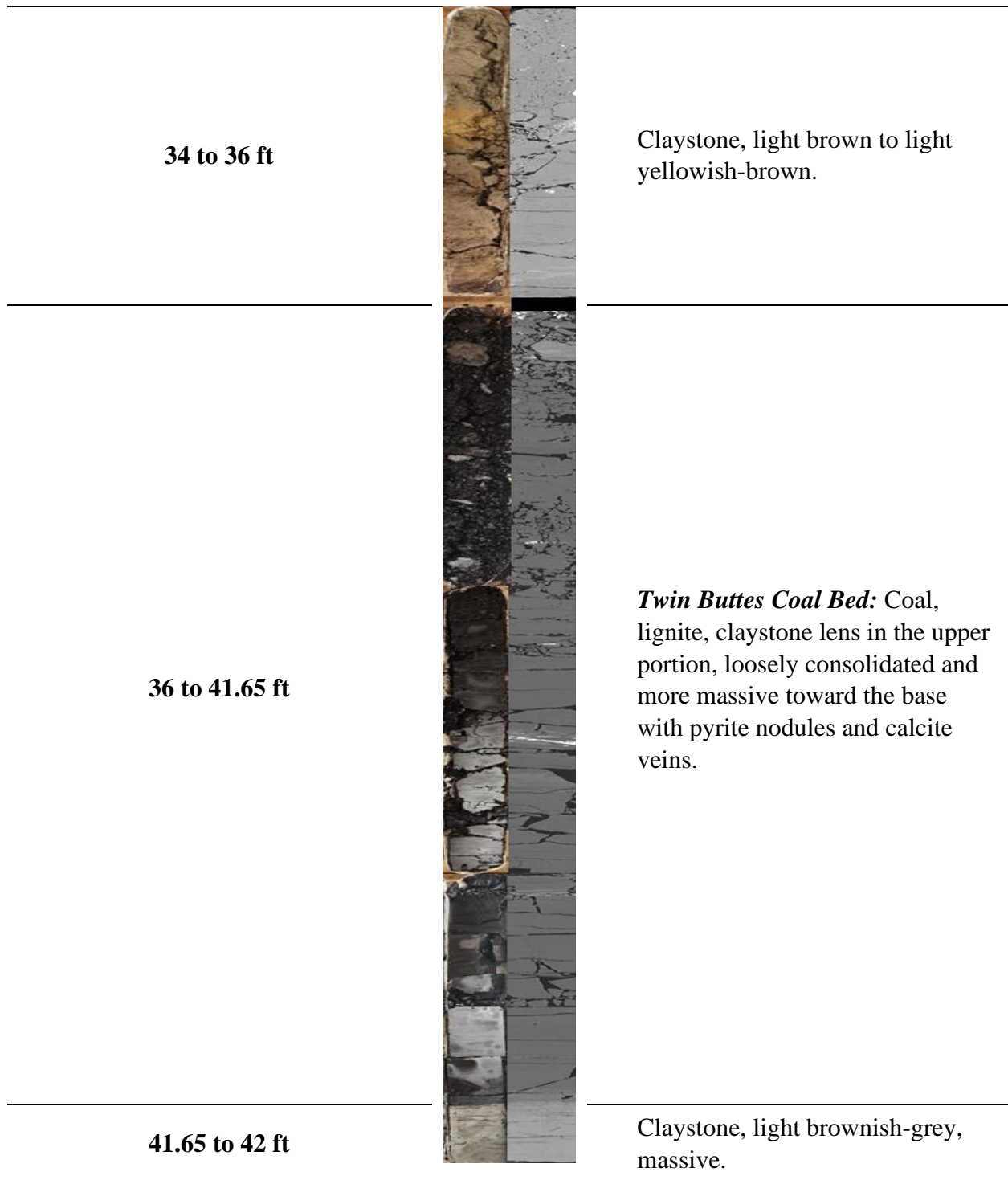


Figure 2: Core photos, medical CT images, and stratigraphic description for the MC23080C well.

Hagel Coal Bed– 23-B001 Well (1 of 2)



Figure 3: Core photos, medical CT images, and stratigraphic description for the 23-B001 well (1 of 2).

Hagel Coal – 23-B001 Well (2 of 2)

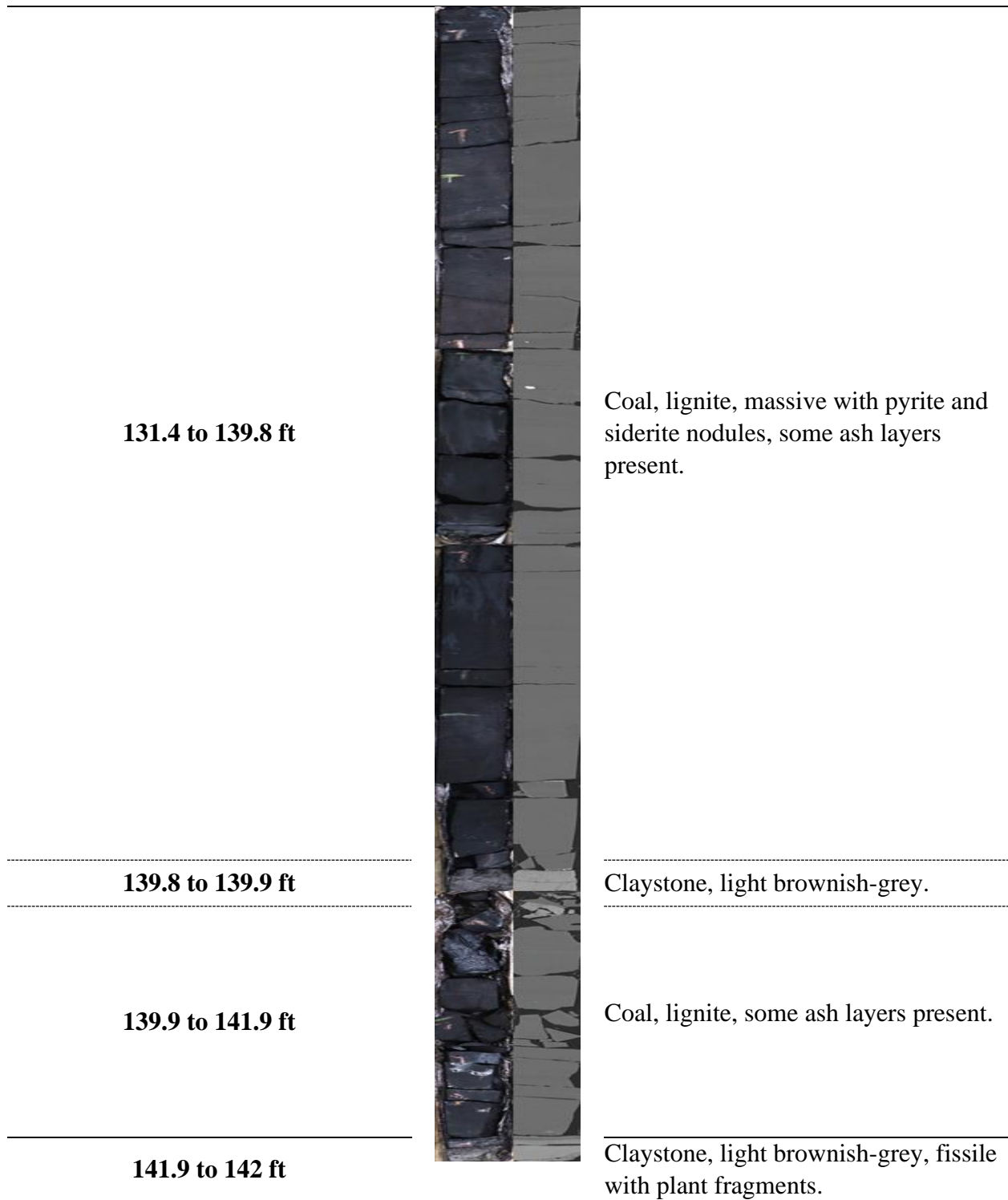


Figure 4: Core photos, medical CT images, and stratigraphic description for the 23-B001 well (2 of 2).

2. DATA ACQUISITION AND METHODOLOGY

The core was evaluated using medical CT scanning and high spatial resolution geophysical measurements along its length, including X-ray fluorescence (XRF) spectrometry.

2.1 MEDICAL CT SCANNING

Core scale CT scanning was performed with a Toshiba Aquilion TSX-101A/R medical CT scanner shown in Figure 5. The medical CT scanner generates images with a resolution in the millimeter range, with scans having voxel resolutions of 0.43 x 0.43 mm in the XY plane and 0.50 mm along the core's long axis (i.e., z-axis). The scans were conducted at a voltage of 135 kV and at a current of 200 mA. Subsequent processing and combining of stacks were performed to create three-dimensional (3D) volumetric representations of the cores and a two-dimensional (2D) cross-section through the middle of the core samples using ImageJ, an open-source image processing software package (Schneider et al., 2012). The variation in greyscale values observed in the CT images indicates changes in the CT number (CTN) obtained from the CT scans, which is directly proportional to changes in the attenuation and density of the scanned rock; darker regions are less dense. Filled fractures, open fractures, and changes in bedding structure can all be resolved via careful examination of the CT images (Figure 11 to Figure 13). While the medical CT scanner was not used for detailed characterization in this study, it allowed for non-destructive bulk characterization of the core.



Figure 5: Toshiba Aquilion Multislice Helical CT scanner at NETL used for core analysis.

2.2 INDUSTRIAL CT SCANNING

High-resolution CT scans were performed on intervals of interest using NETL's North Star Imaging Inc. M-5000[®] Industrial CT System (Figure 6). The system is used to obtain higher resolution scans, resolving some unclear features from the medical scans. NETL's North Star Imaging Inc. M-5000[®] was used to obtain 2D radiographs of the samples 1,440 times while rotating 360°, or at every 0.25°. Radiographs were comprised of four images averaged with a 0.5 s acquisition for each image to ensure sufficient image contrast.

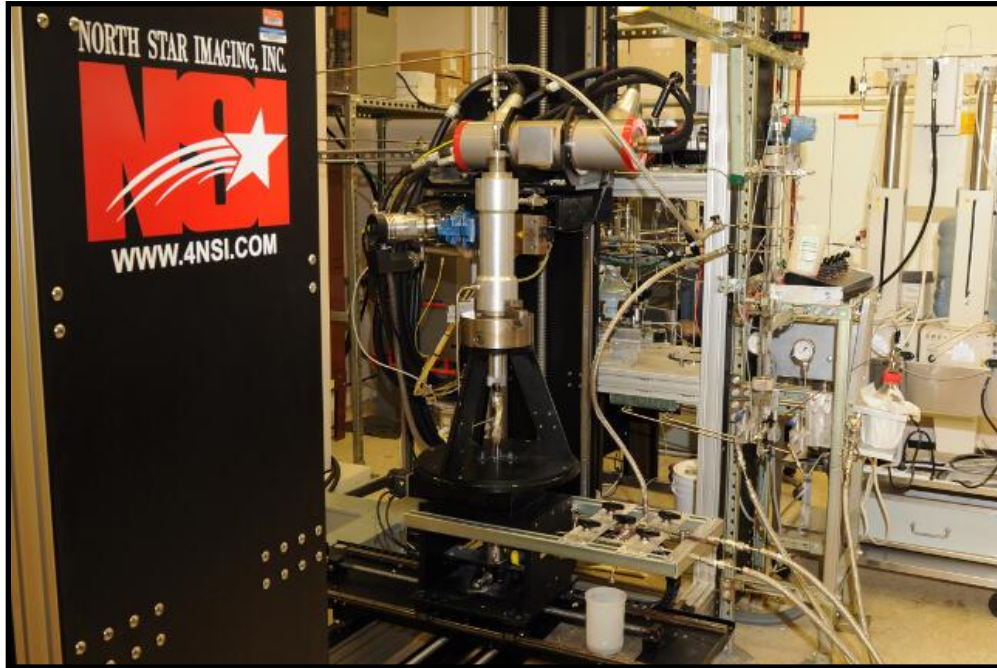


Figure 6: North Star Imaging Inc. M-5000[®] Industrial CT Scanner at NETL used for core analysis.

2.3 MICRO-CT SCANNING

Micro-CT scanning was performed using two scanners at NETL, the TESCAN DynaTOM micro-CT scanner and the ZEISS Xradia MicroXCT-400 scanner.

The DynaTOM performs both, dynamic and static imaging while capturing scans of sub-mm to cm-scale samples (Figure 7). The Xradia system has the highest resolution of the scanners at NETL and scans samples sizes from sub-mm to 25 mm (Figure 8). Both scanners provide detailed image data that can be used to infer porosity, mineralogy, and structure.

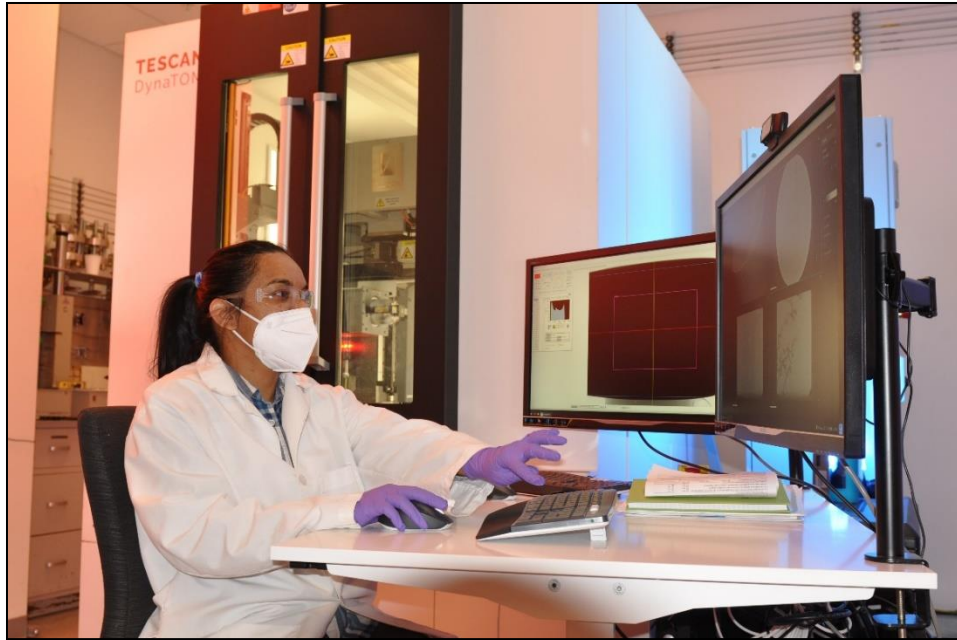


Figure 7: TESCAN DynaTOM Micro-CT scanner used for high-resolution CT imaging at NETL.



Figure 8: Zeiss Xradia MicroXCT-400 Micro-CT scanner used for high-resolution CT imaging at NETL.

2.4 CORE LOGGING

Geophysical measurements of magnetic susceptibility and attenuated gamma counts were obtained with a Geotek® MSCL system on competent sections of the cored intervals and are reported in Section 3.4. Additionally, the system measured bulk elemental chemistry using a built-in, portable XRF spectrometer. The compiled core logs were scaled to fit on single pages for rapid review of the combined data from the medical CT scans and XRF readings.

2.4.1 Magnetic Susceptibility

Magnetic susceptibility is a measure of the degree of magnetization in a sample. The sample is exposed to an external magnetic field and magnetic susceptibility is its measured magnetic response to that field:

$$J = kH$$

Where, J is the magnetic response (per unit volume), k is volume susceptibility, and H is an external magnetic field. The measurement unit is dimensionless (abbreviated as SI).

All materials have magnetic susceptibility. Positive values of magnetic susceptibility indicate that materials are *paramagnetic* and occur in rocks that consist of the majority ferromagnetic, ferrimagnetic, or antimagnetic (iron-bearing) materials. Negative values of magnetic susceptibility indicate that materials are *diamagnetic* and occur in rocks dominated by non-iron materials (e.g., calcite or quartz). Table 2 lists examples of common magnetic susceptibility ranges (Hunts et al., 1995).

Magnetic susceptibility was measured using the Bartington point sensor, where a 1-cm diameter, low intensity (8.0 A/m RMS), non-sensitive, alternating magnetic field (2 kHz) was generated for 10 s. To minimize any potential drift in the oscillating field, the point sensor was zeroed at the beginning and end of the sample and after every fifth measurement. The point sensor, due to the small field, was limited in whole core measurements and was temperature dependent (Geotek Ltd. Multi-Sensor Core Logger Manual, Version 05-10; Geotek Ltd., 2010).

Table 1: Magnetic Susceptibility Values for Common Minerals (Hunts et al., 1995)

Mineral	$\times (*10^{-6})$ SI
Water	9
Calcite	-7.5 to -39
Halite, Gypsum	-10 to -60
Shale	63 to 18,600
Illite, Montmorillonite	330 to 410
Pyrite	5 to 3,500
Chalcopyrite	23 to 400
Hematite	500 to 40,000
Magnetite	1,000,000 to 5,700,000

2.4.2 Gamma Density

Gamma density was acquired by subjecting the sample to gamma radiation and then measuring the attenuation of that radiation. The attenuation is directly proportional to the density of the sample and is acquired by measuring the difference between radiation energy at the emission source and after it passes through the sample. Specifically, the MSCL software calculates the bulk density, ρ , by using the following equation:

$$\rho = \left(\frac{1}{\mu d}\right) \ln\left(\frac{I_o}{I}\right)$$

Where μ = Compton attenuation coefficient, d = sample thickness, I_o = source intensity, and I = measured intensity.

2.4.3 XRF Spectrometry

In addition to the geophysical measurements, a portable handheld Olympus Vanta M Series XRF Spectrometer was used to measure relative elemental abundances of aggregated “light elements” up to and including sodium, and various “heavy elements” which were measured individually. Elemental abundances are reported in ppm relative to the total elemental composition (i.e., the total XRF counts).

The XRF spectrometer measures elemental abundances by subjecting the sample to X-ray photons. The high energy of the photons displaces inner orbital electrons in the respective elements. The vacancies in the lower orbitals cause outer orbital electrons to “fall” into lower orbits to satisfy the disturbed electron configuration. The substitution into lower orbitals causes a release of a secondary X-ray photon, which has an energy associated with a specific element. These relative and element specific energy emissions can then be used to determine bulk elemental composition.

The Olympus Vanta M Series XRF Spectrometer used a “GeoChem(3-beam) Mode” to run at 30.48 cm (1 ft) resolution for 120 s exposure time analysis (40 s per beam). The GeoChem(3-beam) Mode utilizes a three-beam analysis that resolves major (Mg, Al, Si, P, S, Fe, K, Ca, and Ti), minor (V, Cu, Ni, Cr, Mn, Ba, Sr, and Pb), and trace elements (Co, Zn, As, Zr, Mo, Ag, Cd, Sn, Sb, Hg, W, Th, U, and Bi), and some rare earth elements (Y, Ce, La, Pr, and Nd) (orange, Figure 9). The system also resolves an aggregated “light element” (H to Na) (green, Figure 9).

PERIODIC TABLE OF THE ELEMENTS

1 H Hydrogen 1.008																	2 He Helium 4.003
3 Li Lithium 6.941	4 Be Beryllium 9.012											5 B Boron 10.811	6 C Carbon 12.011	7 N Nitrogen 14.007	8 O Oxygen 15.999	9 F Fluorine 18.998	10 Ne Neon 20.180
11 Na Sodium 22.990	12 Mg Magnesium 24.305											13 Al Aluminum 26.982	14 Si Silicon 28.086	15 P Phosphorus 30.974	16 S Sulfur 32.065	17 Cl Chlorine 35.453	18 Ar Argon 39.948
19 K Potassium 39.098	20 Ca Calcium 40.078	21 Sc Scandium 44.956	22 Ti Titanium 47.867	23 V Vanadium 50.942	24 Cr Chromium 51.996	25 Mn Manganese 54.938	26 Fe Iron 55.845	27 Co Cobalt 58.933	28 Ni Nickel 58.693	29 Cu Copper 63.546	30 Zn Zinc 65.390	31 Ga Gallium 69.723	32 Ge Germanium 72.640	33 As Arsenic 74.922	34 Se Selenium 78.960	35 Br Bromine 79.904	36 Kr Krypton 83.800
37 Rb Rubidium 85.468	38 Sr Strontium 87.620	39 Y Yttrium 88.906	40 Zr Zirconium 91.224	41 Nb Niobium 92.906	42 Mo Molybdenum 95.939	43 Tc Technetium 98.000	44 Ru Ruthenium 101.070	45 Rh Rhodium 102.905	46 Pd Palladium 106.420	47 Ag Silver 107.868	48 Cd Cadmium 112.411	49 In Indium 114.818	50 Sn Tin 118.710	51 Sb Antimony 121.760	52 Te Tellurium 127.600	53 I Iodine 126.905	54 Xe Xenon 131.293
55 Cs Cesium 132.905	56 Ba Barium 137.327	57-71 La-Lu Lanthanides	72 Hf Hafnium 178.490	73 Ta Tantalum 180.948	74 W Tungsten 183.840	75 Re Rhenium 186.207	76 Os Osmium 190.230	77 Ir Iridium 192.222	78 Pt Platinum 195.078	79 Au Gold 196.967	80 Hg Mercury 200.590	81 Tl Thallium 204.383	82 Pb Lead 207.200	83 Bi Bismuth 208.980	84 Po Polonium 209.000	85 At Astatine 210.000	86 Rn Radon 222.000
87 Fr Francium 223.000	88 Ra Radium 226.000	89-103 Ac-Lr Actinides	104 Rf Rutherfordium 261.000	105 Db Dubnium 262.000	106 Sg Seaborgium 266.000	107 Bh Bohrium 264.000	108 Hs Hassium 277.000	109 Mt Meitnerium 278.000	110 Ds Darmstadtium 281.000	111 Rg Roentgenium 282.000	112 Cn Copernicium 285.000	113 Nh Nihonium 286.000	114 Fl Flerovium 289.000	115 Mc Moscovium 290.000	116 Lv Livermorium 293.000	117 Ts Tennessine 294.000	118 Og Oganesson 294.000
57 La Lanthanum 138.905	58 Ce Cerium 140.116	59 Pr Praseodymium 140.908	60 Nd Neodymium 144.240	61 Pm Promethium 144.913	62 Sm Samarium 150.360	63 Eu Europium 151.964	64 Gd Gadolinium 157.250	65 Tb Terbium 158.925	66 Dy Dysprosium 162.500	67 Ho Holmium 164.930	68 Er Erbium 167.259	69 Tm Thulium 168.934	70 Yb Ytterbium 173.054	71 Lu Lutetium 174.967			
89 Ac Actinium 227.000	90 Th Thorium 232.038	91 Pa Protactinium 231.036	92 U Uranium 238.029	93 Np Neptunium 237.000	94 Pu Plutonium 244.000	95 Am Americium 243.000	96 Cm Curium 247.000	97 Bk Berkelium 247.000	98 Cf Californium 251.000	99 Es Einsteinium 252.000	100 Fm Fermium 257.000	101 Md Mendelevium 258.000	102 No Nobelium 259.000	103 Lr Lawrencium 262.000			

Figure 9: Periodic table showing elements (colored) measurable by the Olympus Vanta M Series XRF Spectrometer using the “GeoChem(3-beam)” mode.

2.5 DATA COMPILATION

Strater[®] by Golden Software was used to compile the medical CT data into a series of logs. The data used to generate these logs can be accessed from NETL's [EDX](https://edx.netl.doe.gov/dataset/eerc_corecm_williston_basin_cores) using the following link: https://edx.netl.doe.gov/dataset/eerc_corecm_williston_basin_cores.

3. RESULTS

The following sections contain the data obtained from the medical and industrial CT scanners, in addition to the MSCL scans, of the cored intervals.

3.1 MEDICAL CT SCANS

Processed 2D slices of the medical CT scans through the cores are shown. As discussed previously, the variation in greyscale values observed in the medical CT images indicates changes in the CTN obtained, which is directly proportional to changes in the attenuation of the X-ray beam, and thus density of the scanned rock (i.e., darker regions are less dense, lighter regions are denser).

3.1.1 XZ Planes

A 2D image through the center of each core can be found in Figure 11 through Figure 13. These are referred to as “XZ” planes with the coordinates that are shown in Figure 10. Each image has a red 2-cm scale bar; the core diameter is 2.5 in. The labels below each 2D XZ plane in Figure 11 through Figure 13 are the depth of each core. Due to the contrast difference between the coal seams and the surrounding rock two images of each section are shown.

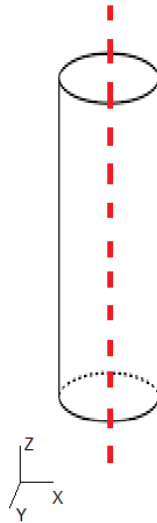


Figure 10: Schematic of the XZ isolated plane through the vertical center of the medical CT scans.

3.1.2 23-B001 Well

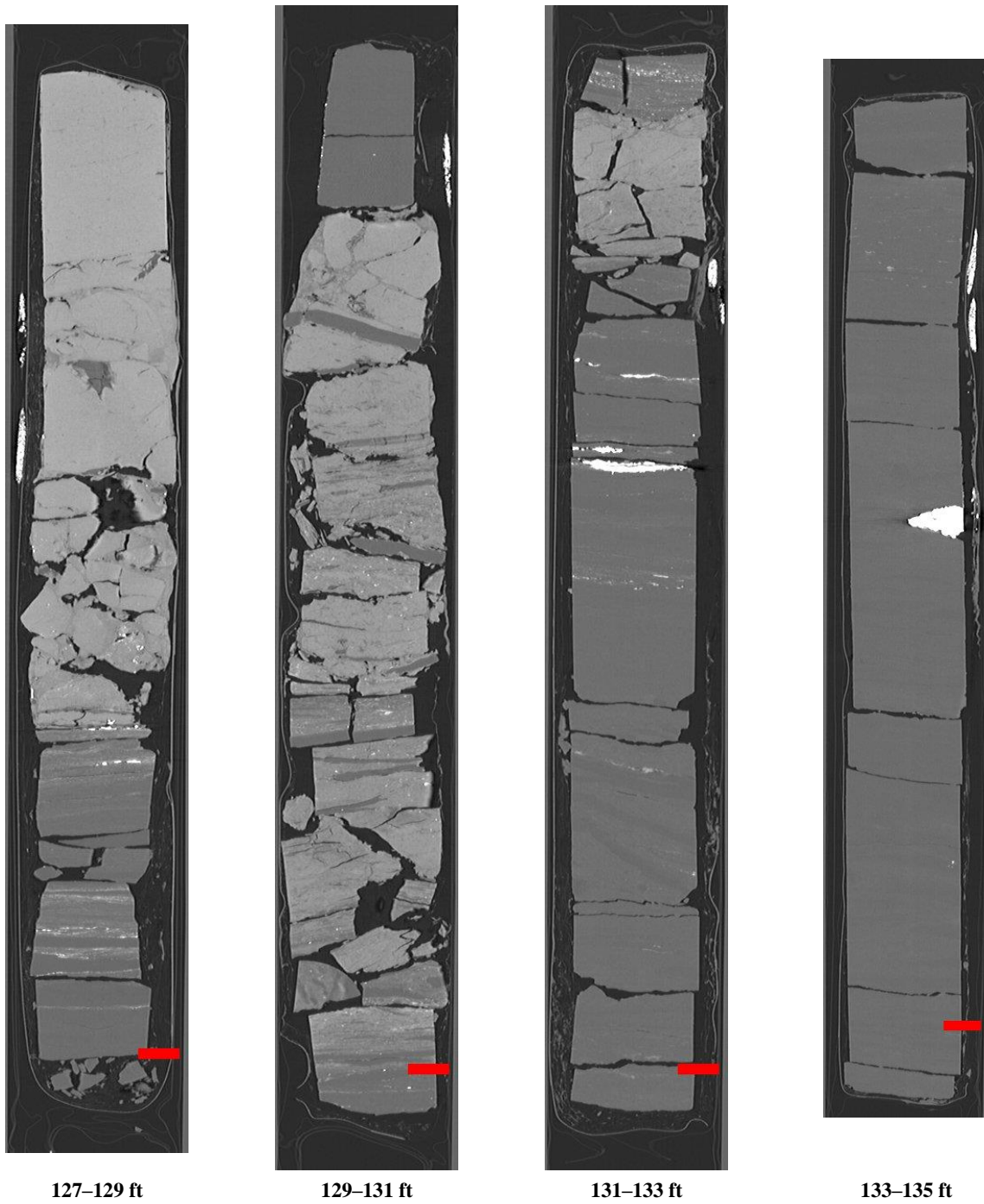


Figure 11: 2D isolated planes through the vertical center of the medical CT scans of the 23-B001 well from 127-135 ft.

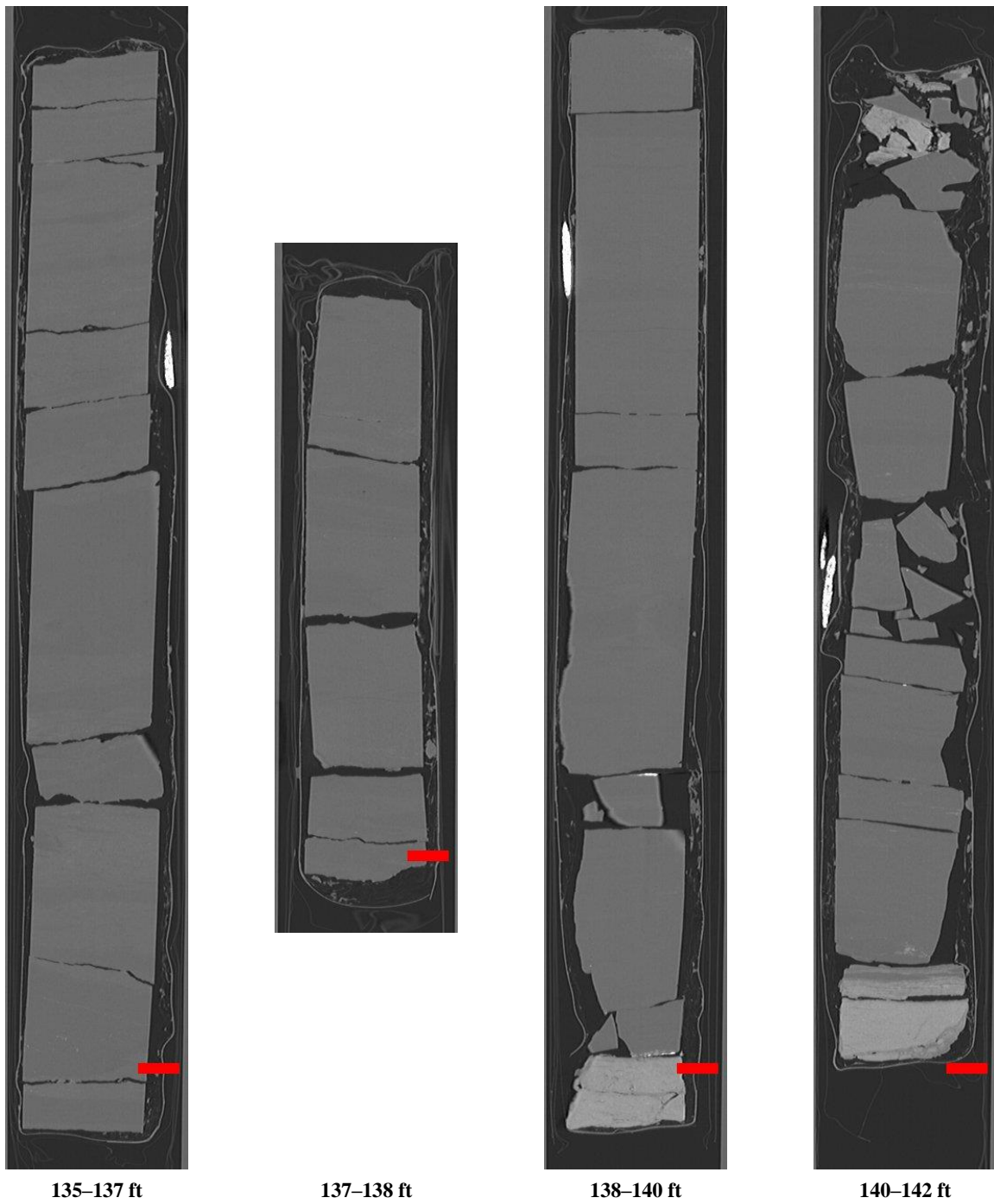


Figure 12: 2D isolated planes through the vertical center of the medical CT scans of the 23-B021 well from 135-142 ft.

3.1.3 MC23080C Well

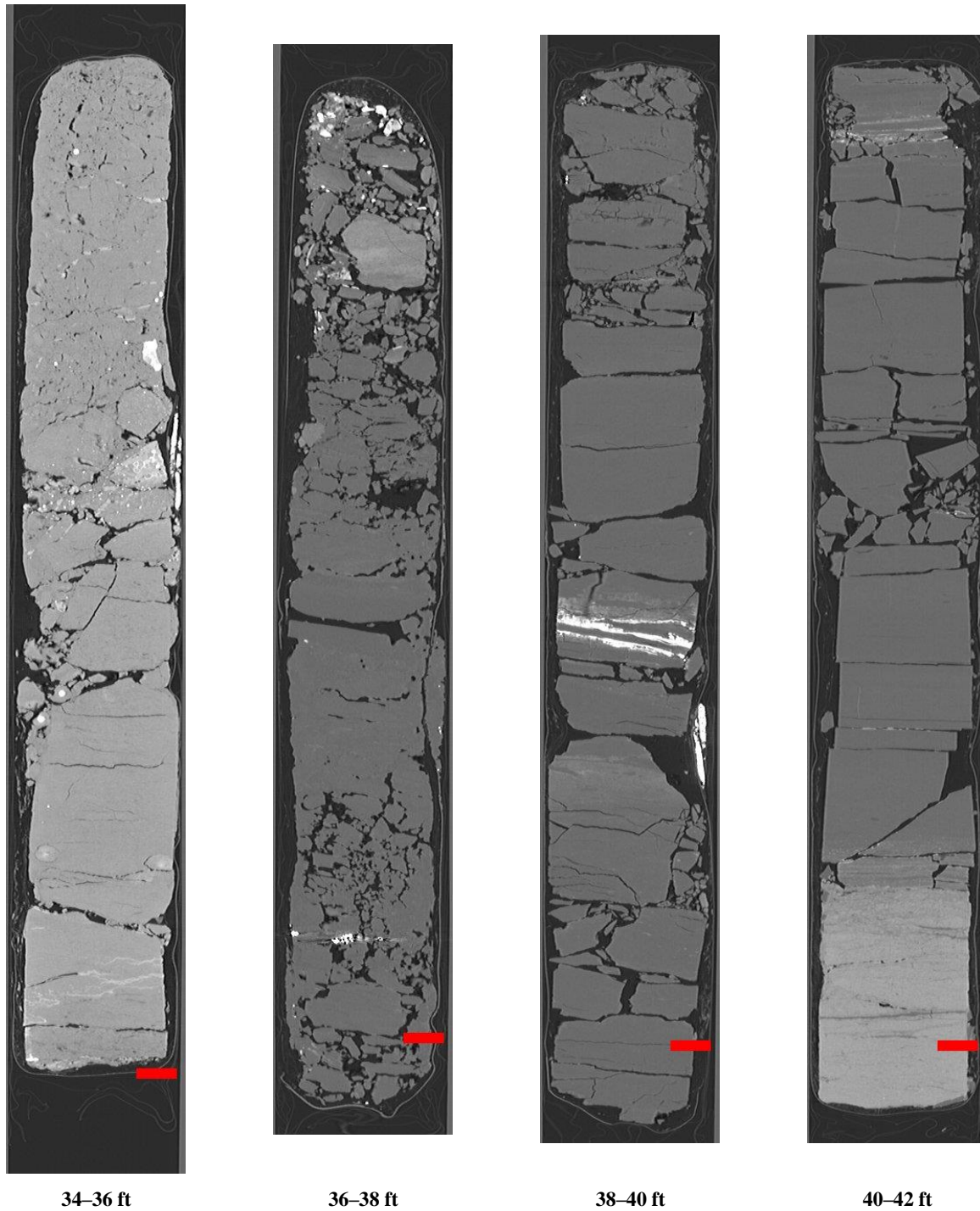


Figure 13: 2D isolated planes through the vertical center of the medical CT scans of the MC23080C well from 34-42 ft.

3.2 ADDITIONAL CT DATA

Additional CT data can be accessed from NETL's [EDX](#) using the following link: https://edx.netl.doe.gov/dataset/eerc_corecm_williston_basin_cores. The original CT data is available as 16-bit TIF stacks suitable for reading with ImageJ (Schneider et al., 2012) or other image analysis software.

3.2.1 Medical CT Image Videos

In addition, videos showing the variation along the length of the cross-section images shown in the previous section are available for download and viewing on EDX. A single image from these videos is shown in Figure 14, where the cross-section of MC23080C well core from 38–42 ft displays high attenuating bedding. The videos on [EDX](#) show this XY variation along the entire length of the core.

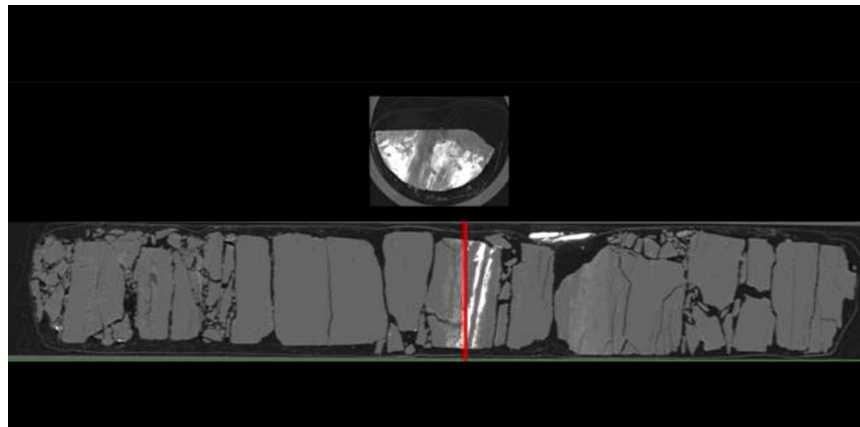


Figure 14: Single image from a video file available on EDX showing variation in the MC23080C well core from 38–42 ft. Image above shows the variation in composition within the matrix perpendicular to the core length. The red line through the XZ-plane image of the core shows the location of the XY-plane displayed above.

3.2.2 Industrial CT Scans

Detailed scans of sections of interest were performed by the NorthStar Imaging Inc. M-5000® Industrial Computed Tomography System (Industrial CT) at NETL. The system was used to obtain a higher resolution scan with voxel resolution at $10.5 \mu\text{m}^3$ (Table 2) and capture the details of certain features clearly. The whole core scans were performed at a voltage of 165 kV and a current of $300 \mu\text{A}$. These settings provided the appropriate photon energy to penetrate the samples. The samples were rotated 360° and 1,440 radiograph projections of the samples were obtained, averaging four individual radiographs at each step to create the reconstruction. Resampled images illustrating the variation along the length of each volume are shown in Figure 15.

Table 2: Industrial Scans from Whole Core, All Available on EDX

Depth (ft)	File Name	Resolution (μm^3)
140.6	Hagel_140.6_Lignite	10.5

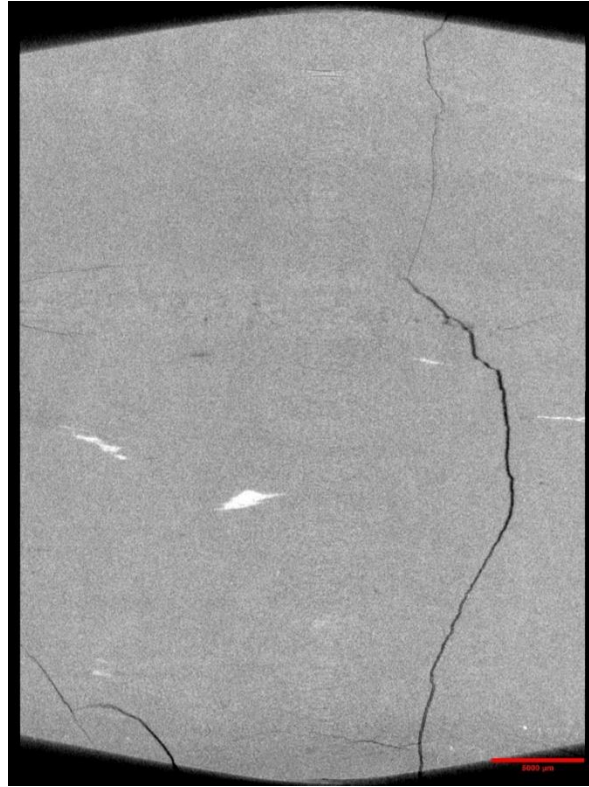


Figure 15: 2D isolated planes through the vertical center of the industrial CT scans of the 23-B001 well from 140.6 ft. Red scale bar is 5 mm.

3.2.3 Micro-CT scans

Detailed micro-CT scans of mm-scale subcores from select regions were performed at NETL. The micro-CT scanners discussed in Section 2.3 were used to obtain higher resolution images and capture the details of internal features. A list of the core sections scanned with the micro-CT scanners are shown in Table 3 and Table 4 for the Xradia and DynaTOM scanners, respectively, followed by images from these scanned volumes along the XY planes of these samples. Resampled images representing each volume are shown in Figure 16 and Figure 17. Full 3D TIF stacks of this data is available on https://edx.netl.doe.gov/dataset/eerc_corecm_williston_basin_cores.

Table 3: Overview of Available Micro-CT Scans, All Available on EDX

Depth (ft)	File Name	Resolution (μm^3)
141.95	Hagel_141.95_4x	1.68
141.95	Hagel_141.95_M70	4.42
139.8	Hagel_139.8_4x	1.68
139.8	Hagel_139.8_M70	4.42
141	Hagel_A_141_4x	1.68
141	Hagel_A_141_M70	4.42

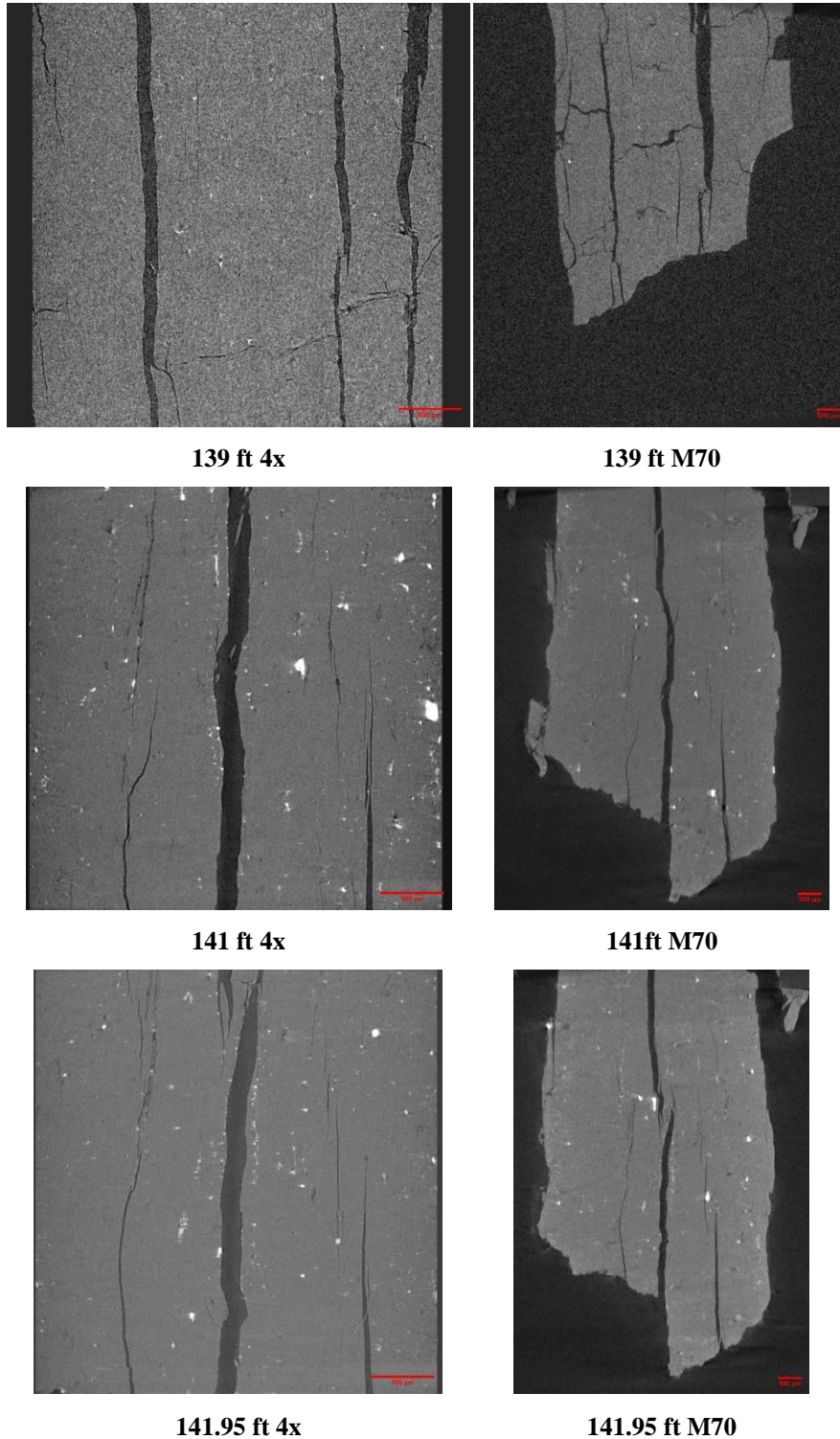


Figure 16: 2D isolated planes through the vertical center of the Xradia micro-CT scans of the 23-B001 well from 139 ft to 141.95 ft. 4x scans have a voxel resolution of $1.68 \mu\text{m}^3$ and M70 have a voxel resolution of $4.42 \mu\text{m}^3$. Red scale bars are 500 microns.

Table 4: DynaTOM Micro Scans, All Available on EDX

Depth (ft)	File Name	Resolution (μm^3)
139.8	Hagel_139.8	22.37
141	Hagel_141	15.25

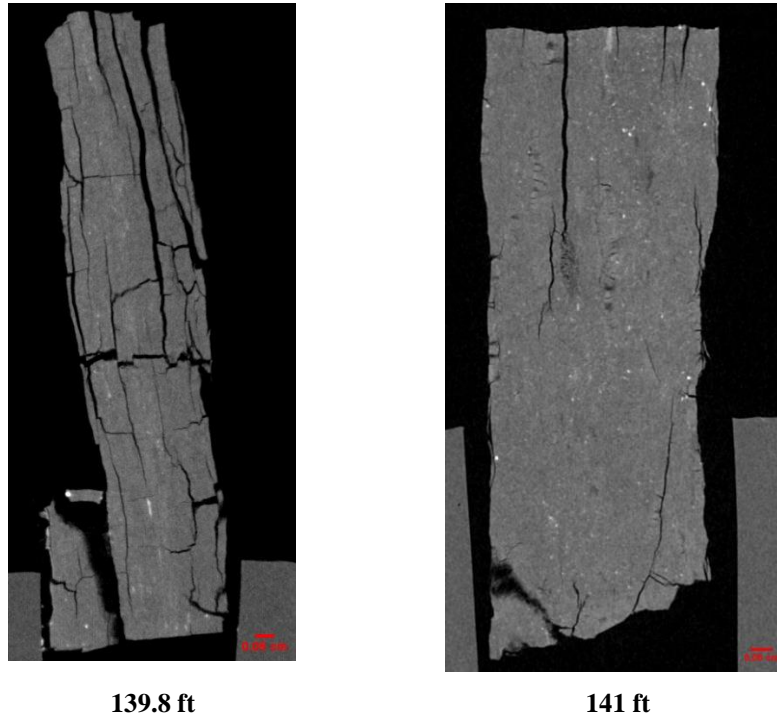


Figure 17: 2D isolated planes through the vertical center of the micro-CT scans of the 23-B001 well from 139.8 ft and 141 ft. Red scale bars are 0.5 mm.

3.3 DUAL ENERGY CT SCANNING

Dual energy CT scanning uses two sets of images, produced at different X-ray energies, to approximate the density (ρ_B) (Siddiqui and Khamees, 2004; Johnson, 2012). The technique relies on the use of several standards of known ρ_B to be scanned at the same energies as the specimen. These scans are performed at lower energies (<100 KeV) and higher energies (>100 KeV) to induce two types of photon interactions with the object (Figure 18). The lower energy scans induce photoelectric absorption, which occurs when the energy of the photon is completely absorbed by the object mass and causes ejection of an outer orbital electron (Figure 18a). The high energy scans induce Compton scattering, which causes a secondary emission of a lower energy photon due to incomplete absorption of the photon energy in addition to an electron ejection (Figure 18b).

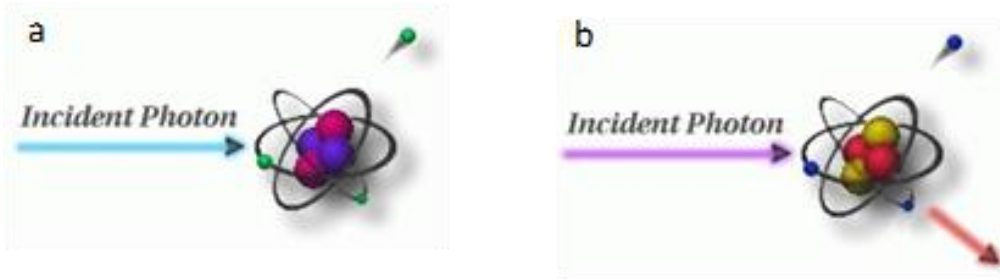


Figure 18: Photon interactions at varying energies: a) Photoelectric absorption, b) Compton scattering. Modified from Iowa State University Center for Nondestructive Evaluation (2021).

Medical grade CT scanners are typically calibrated to known standards, with the output being translated in CTN or Hounsfield Units (HU). Convention for HU defines water as 0 and air as -1,000. A linear transform of recorded HU values is performed to convert them into CTN. This study used CTN as it is the native export format for the medical CT scanner, but it is possible to use HU. Dual energy CT requires at least three calibration points, and it is prudent to utilize standards that approximate the object or material of interest. Pure samples of aluminum, graphite, and sodium chloride were used as the calibration standards as they most closely approximate the rocks and minerals of interest (Table 5). Most materials denser than water or with higher atomic masses have a non-linear response to differing CT energies (Table 6).

Table 5: Dual Energy Calibration Standards, Bulk Density (gm/cm³)

Material	ρ_B (g/cm ³)
Air	-0.001
Water	1
Graphite	2.3
Sodium Chloride	2.16
Aluminum	2.7

Table 6: Dual Energy Calibration Standards, HU and CTN for “Low” and “High” Energies

Material	HU		CTN	
	80 KeV	135 KeV	80 KeV	135 KeV
Air	-993	-994	31,775	31,774
Water	-3.56	-2.09	32,764	32,766
Graphite	381	437	33,149	33,205
Sodium Chloride	1,846	1,237	34,614	34,005
Aluminum	2,683	2,025	35,451	34,793

Dual energy CT utilizes these differences to calibrate to the X-ray spectra. Two equations with three unknowns each are utilized to find ρ_B (Siddiqui and Khamees, 2004):

$$\rho_B = mCTN_{low} + pCTN_{high} + q$$

Where [m, p, and q] are unknown coefficients that can be solved by setting up a system of equations with four 3×3 determinants. The CTN is obtained from the CT scans for each of the homogenous calibration standards.

In this study, the high and low energy image stacks were loaded into Python as arrays. A 3D Gaussian blur filter with a sigma of 2 was used to reduce noise in the images. The `scipy.solve` module of Python was then employed to solve for the coefficients based on the calibration CTN values. The ρ_B was solved for each pixel in the 3D volume and saved as two new separate image stacks.

3.4 COMPILED CORE LOG

The compiled core logs were scaled to fit on single pages for rapid review of the combined data from the medical CT scans and MSCL readings. Logs are presented for each of the cored sections from the 23-B001 and MC23080C wells. Both cores were run at 6 cm and focused high spatial resolution scanning at 2 cm intervals (23-B021: 127 to 136 ft; MC23080C: 36 to 42 ft).

All available cores were medically CT scanned. Each log includes the following tracks: track 1, dual energy density (ρ ; g/cm^3); track 2, elemental XRF mineralogy that are colored to indicate carbonates (blue, Mg + Ca), quartz (yellow, Si), clays (grey, Al; red, Fe; pink, K), and sulfuric minerals (gold, S); track 3, medical CT images, cropped to center portion of images to highlight greyscale variations; track 4, 5, 6, 7, and 8 proxy elemental measurements in parts per million; and track 9 shows a summation of rare earth elements (REE) elements (La, Ce, and Y) that may lead as a proxy for enrichment in middle and heavy REEs outside of the resolution of the handheld XRF.

The elemental results from the XRF was used to display important elemental proxies related to detrital influence (Si, Al, K, Ti, and Zr in track 4), skeletal influx/carbonate potential (Ca, Mg, Mn, and Ba in track 5), redox potential (V, Cr, Co, Ni, Cu, and Mo in track 6), biogenic production (V, P, Zn, and Y in track 7), and chalcophile (Pb, As, S, and Fe in track 8). Track 9 represents a summation of La, Ce, and Y that can be used to indicate enrichments in REEs.

The elemental proxy log also includes an XRF “mineralogy” with Al and K, representing clays; Ca, representing calcite; and Si, representing quartz, although there is some Si contribution to the clays. Pyrite (reduced) should have low magnetic susceptibility, and Fe oxide or hydroxide should have high magnetic susceptibility. These broad trends can quickly give information over large lengths of core and direct more focused research to zones of potential interest. These logs are presented in the following images (Figure 19 to Figure 20).

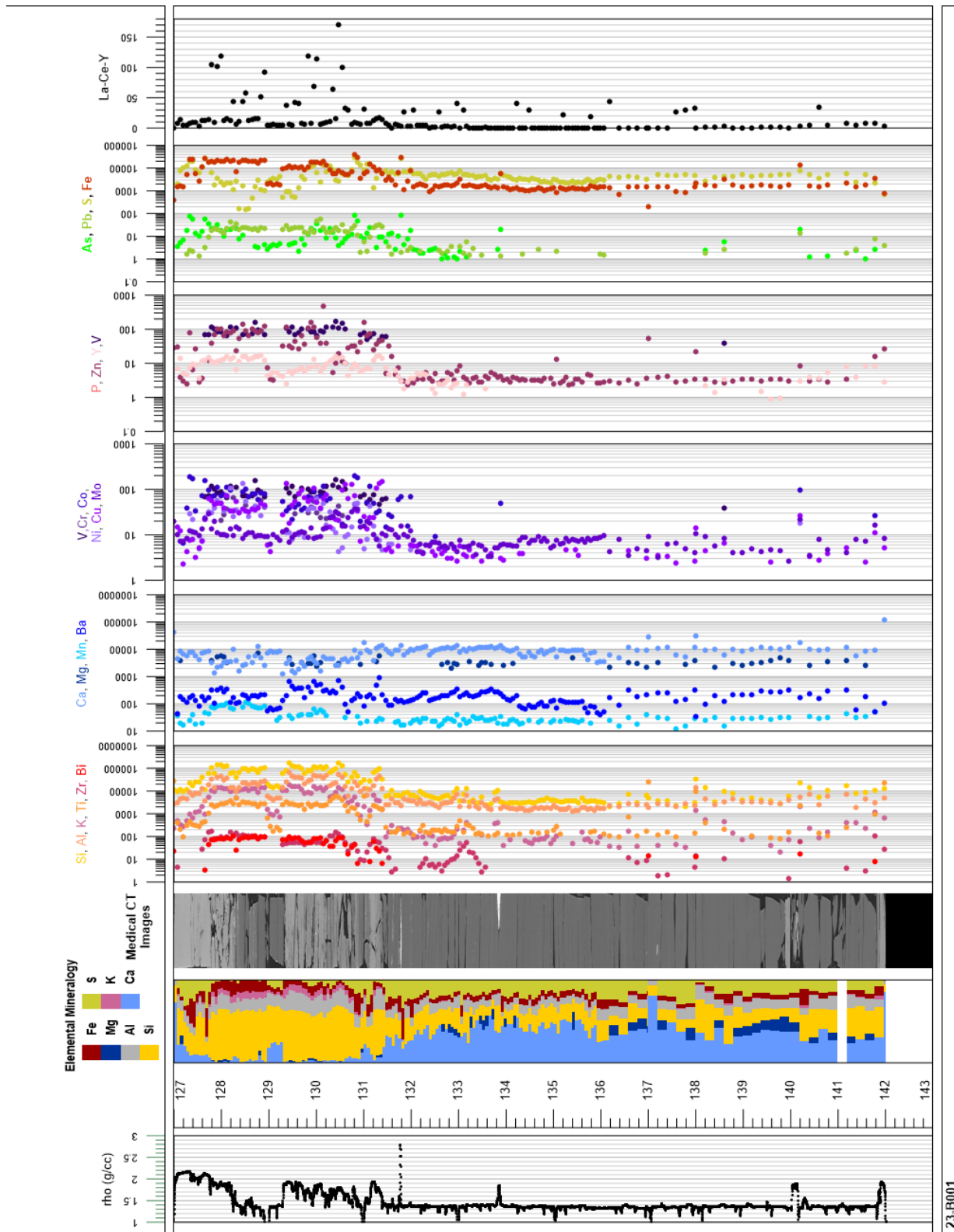


Figure 19: Compiled core log for the 23-B001 well from 127–142 ft.

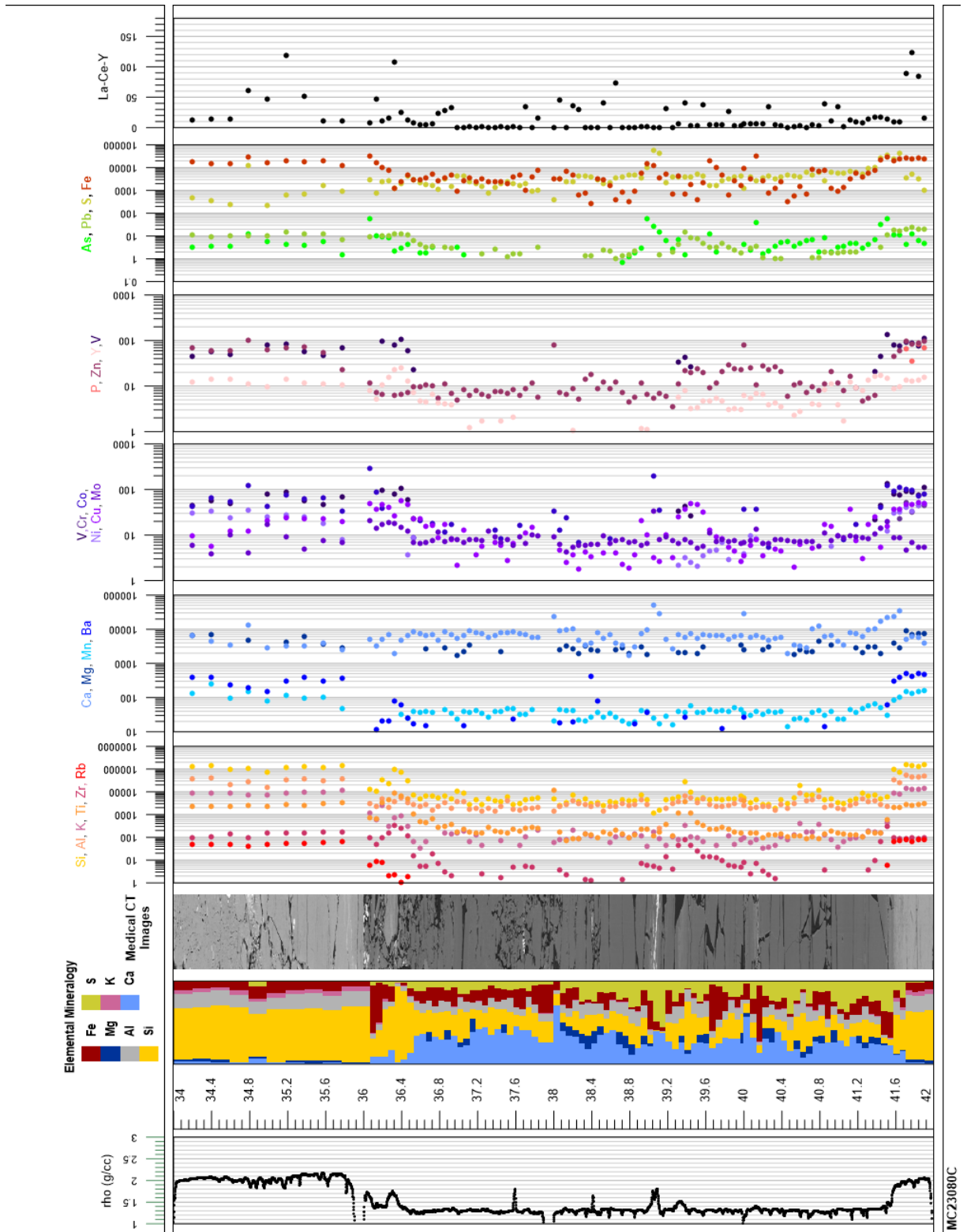


Figure 20: Compiled core log for MC23080C well from 34–42 ft.

4. DISCUSSION

The evaluation of the magnetic susceptibility, elemental XRF, and CT analysis offers a unique look into the internal structure of the core and macroscopic changes in lithology. These methods:

- Are non-destructive
- When employed together, they offer a more thorough understanding of the core than any single technique alone
- Can be used to identify zones of interest for further detailed analysis, experimentation, and quantification, for example:
 - 23-B001 and MC23080C wells shows some enrichments in energy critical elements (V, Cr, Cu, and Zn) in the clays above and below the coal seam; and in a few ash layers within the coals (MC23080C at 40 ft; 23-B001 at 140 ft)
- Provide a detailed digital record of the core, before any destructive testing or further degradation, that is accessible and can be referenced for future studies

This page intentionally left blank.

5. REFERENCES

- Geotek Ltd. Multi-Sensor Core Logger Manual; Version 05-10; Published by Geotek, 3 Faraday Close, Daventry, Northamptonshire NN11 8RD, 2010. info@geotek.co.uk, www.geotek.co.uk
- Hunts, C.; Moskowitz, B.; Banerjee, S. *Magnetic Properties of Rocks and Minerals; Rock Physics and Phase Relations: A Handbook of Physical Constants*; 1995; pp 189–204.
- Iowa State University Center for Nondestructive Evaluation, Ames, IA, 2021. <https://www.nde-ed.org/Physics/X-Ray/attenuation.xhtml> (accessed July 2021).
- Johnson, T. R. C. Dual-Energy CT: General Principles. *American Journal of Roentgenology* **2012**, *199*, S3–S8. DOI: 10.2214/AJR.12.9116.
- Schneider, C. A.; Rasband, W. S.; Eliceiri, K. W. NIH Image to ImageJ: 25 years of image analysis. *Nature Methods* **2012**, *9*, 671–675.
- Siddiqui, S.; Khamees, A. A. Dual-Energy CT-Scanning Applications in Rock Characterization. *Society of Petroleum Engineers* **2004**. DOI:10.2118/90520-MS.

This page intentionally left blank.



Marianne Walck

Director
National Energy Technology Laboratory
U.S. Department of Energy

Jessica Mullen

Critical Minerals Sustainability
Technology Director
National Energy Technology Laboratory
U.S. Department of Energy

Scott Montross

Critical Minerals Sustainability
Technology Director
National Energy Technology Laboratory
U.S. Department of Energy

Anna Wendt

DOE HQ Program Manager
Office of Resource Characterization
U.S. Department of Energy

Bryan Morreale

Associate Laboratory Director of the
Research and Innovation Center
National Energy Technology Laboratory
U.S. Department of Energy